EPJ Photovoltaics **13**, 17 (2022)

https://doi.org/10.1051/epjpv/2022014

Available online at:
www.epj-pv.org

Special Issue on 'Recent Advances in Spectroscopy and Microscopy of Thin-films Materials, Interfaces, and Solar Cells 2021', edited by A. Vossier, M. Gueunier-Farret, J.-P. Kleider and D. Mencaraglia

REGULAR ARTICLE OPEN ACCESS

Investigation of co-evaporated polycrystalline Cu(In,Ga)S_2 thin film yielding 16.0 % efficiency solar cell

Nicolas Barreau[1,*], Eugène Bertin[1,2], Alexandre Crossay[3], Olivier Durand[2], Ludovic Arzel[1], Sylvie Harel[1], Thomas Lepetit[1], Lionel Assmann[1], Eric Gautron[1], and Daniel Lincot[3]

[1] Nantes Université, CNRS, Institut des Matériaux de Nantes Jean Rouxel, IMN, 44000 Nantes, France
[2] Université de Rennes, INSA Rennes, CNRS, Institut FOTON - UMR 6082, 35000 Rennes, France
[3] CNRS, Institut Photovoltaïque d'Île de France, Ecole polytechnique-Institut polytechnique de Paris, Chimie Paristech-PSL, UMR 9006, 91120 Palaiseau, France

Received: 28 March 2022 / Received in final form: 16 May 2022 / Accepted: 23 May 2022

Abstract. The interest for pure sulfide Cu(In,Ga)S_2 chalcopyrite thin films is increasing again because their optical properties make them relevant candidates to be applied as top cell absorbers in tandem structures. Nonetheless, their use as so is still hindered by the level of single-junction cells performance achieved so far, which are far below those demonstrated by selenide absorbers. Amongst the reasons at the origin of the limited efficiency of Cu(In,Ga)S_2-based solar devices, one can mention the poor tolerance of S-chalcopyrite to Cu deficiency. In fact, Cu-poor Cu(In,Ga)S_2 films contain $CuIn_5S_8$ thiospinel secondary phase which is harmful for device performance. In the present work, we investigate Cu(In,Ga)S_2 thin films grown by a modified three-stage process making use of graded indium and gallium fluxes during the first stage. The resulting absorbers are single phase and made of large grains extended throughout the entire film thickness. We propose that such a morphology is a proof of the recrystallization of the entire film during the synthesis. Devices prepared from those films and buffered with bath deposited CdS demonstrate outstanding efficiency of 16.0%. Replacing CdS by Zn(O,S) buffer layer leads to increased open circuit voltage and short circuit current; however, performance become limited by lowered fill factor.

Keywords: Thin film solar cell / wide bandgap / sulfide / CIGS / high efficiency

1 Introduction

Cu(In,Ga)(Se,S)$_2$ compounds with chalcopyrite structure are semiconductors with direct bandgap ranging from 1.0 eV ($CuInSe_2$) through 2.5 eV ($CuGaS_2$) [1]. Such optical properties make those compounds interesting for photovoltaic applications. During the last decade, outstanding level of performance has been achieved with pure selenides (22.6% [2]) and sulfo-selenides (23.4% [3]) polycrystalline thin film as absorber layer. Regarding devices based on pure sulfides, though record efficiency did not exceed 16% [4–6], they recently gained renewed interest for their possible application as top cell in tandem structures [7].

Devices demonstrating efficiencies higher than 12% have been fabricated from Cu(In,Ga)S_2 polycrystalline thin films synthesized by either the annealing of stacked elemental layer [4,8] or sequential co-evaporation [5,6]. In contrast to selenides, the pseudo ternary phase diagram of sulfides suggests a much narrower domain where single phased chalcopyrite material is formed [9]. In particular, even slight Cu deficiency relative to 1-1-2 (Cu-III-S) stoichiometry leads to the spontaneous formation of thiospinel $CuIn_5S_8$-like secondary phase, which is known as detrimental for device performance [10]. Therefore, it is crucial to control finely the composition of the films during their whole synthesis process to expect achieving high efficiency.

So far, the co-evaporation process leading to the best performance is the sequential 3-stage process. However, as recently reported [6,11] its implementation can result in the formation of bi-layered films corresponding to two different indium and gallium contents. In fact, a major part of the gallium is found at the half-rear part of the film (*i.e.* forming $CuIn_{0.1}Ga_{0.9}S_2$), whereas indium is found towards half-top section (i.e. forming $CuIn_{0.9}Ga_{0.1}S_2$). Such compositional separation into bi-plateau structure is likely to alter films optoelectronic characteristics for photovoltaic applications.

The present work aims at investigating a modified three-stage process expected to favor the achievement of

* e-mail: nicolas.barreau@univ-nantes.fr

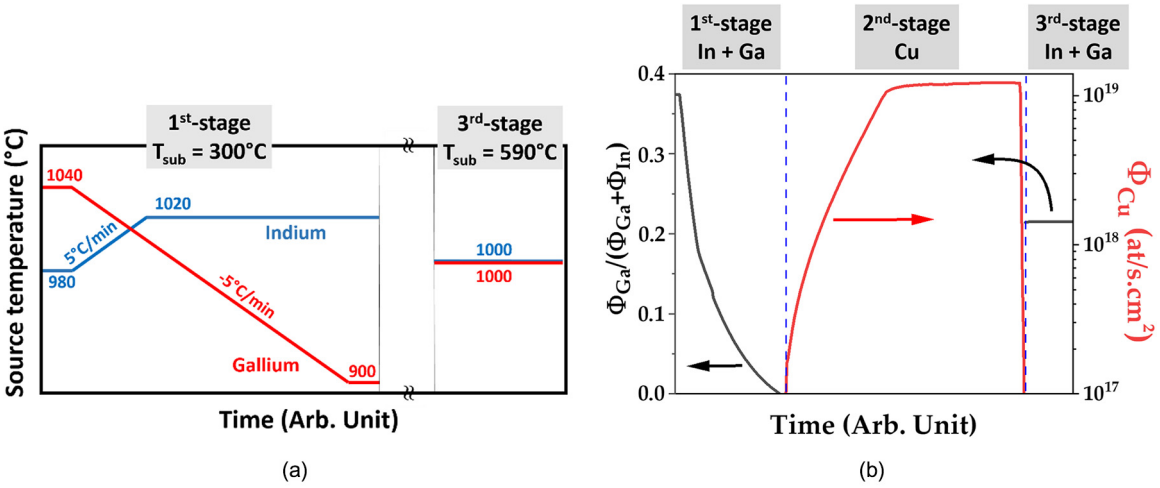

Fig. 1. (a) Variations (not to scale) of indium (in blue) and gallium (in red) source temperatures during the first and the third stage of the implemented process. (b) Evolution of atom fluxes calculated from calibration curves (i.e. rate versus source temperature). In black is represented the ratio of group III atom fluxes during the first and third stage; in red is plotted the evolution of Cu atom flux during the second stage.

much smoother transition between rear and front side compositions. The approach we propose consists in varying the indium and gallium atom fluxes supplied during the first stage of the process, keeping all other process parameters similar. The manuscript is structured as follows: after giving a detailed description of the modified process, we report on the characteristics of the films achieved at the end of the first stage; then, those of the completed absorber. In a following section, we present the characteristics of the solar cells fabricated from those absorbers and buffered with CdS. Finally, we compare the performance of devices with either CdS or Zn(O,S) buffer layer.

2 Experimental

2.1 Thin film growth

$Cu(In,Ga)S_2$ thin films are deposited following the so-called 3-stage process, originally developed for pure selenide absorbers [12]. This growth process consists in firstly the evaporation In and Ga under S excess onto soda lime glass (SLG) substrates covered with sputtered molybdenum layer; during this first stage, the substrate temperature is maintained at 300 °C. Secondly, the substrate is heated up and maintained at 590 °C while Cu is supplied under S flux; this second stage ends when the growing film composition turns Cu-rich (i.e. [Cu]/[In]+[Ga] > 1). This Cu-poor/Cu-rich transition is followed during the growth through the change in film emissivity, yielding a sharp increase of the output power of the heating system [13]. Finally, In and Ga are supplied again until the composition of the film turns Cu-poor; this latter transition is also followed during the growth through the decrease of the heating power needed to keep the substrate at 590 °C.

In the present work, the investigated modified process differs from the standard 3-stage regarding the first stage exclusively. In fact, instead of being constant, the fluxes of In and Ga are varied as illustrated in Figure 1a; the temperature of the Ga source is decreased while that of In source is increased. Such source temperature evolutions yield atom flux ratio, namely $\Phi_{Ga}/(\Phi_{Ga}+\Phi_{In})$, decreasing from 0.37 down to 0. This means that at the end of this first stage only In is supplied; a representative evolution during the whole process, deduced from the calibration of each source (i.e. $\Phi_{at.}$ vs. T_{source}) with the help of a quartz deposition balance, is presented in Figure 1b.

2.2 Thin films characterization

The thin films were investigated by X-Ray diffraction (XRD) on a D8 Bruker diffractometer (with a monochromator selecting $CuK_{\alpha 1}$, $\lambda = 1.540598$ Å); peak fitting was conducted with the pseudo-voigt function. Scanning electron microscopy imaging was performed using a JEOL JSM 7600F model. Composition was determined by energy dispersive X-ray spectroscopy using a JEOL JSM 5800LV SEM equipped with a SAMx SDD energy dispersive spectrometer in order to evaluate the mean CGI, i.e. [Cu]/([Ga]+[In]), and GGI, i.e. [Ga]/([Ga]+[In]). Qualitative elements profiling was performed by glow discharge optical emission spectrometry (GDOES) on a GD profiler 2, Horiba.

2.3 Solar cell preparation and characterization

All of the solar cells investigated consist of the following layers stack: SLG/Mo/CIGS/buffer/r-ZnO/ZnO:Al/metallic grids and for the best devices 100 nm of MgF_2 acting as antireflective coating is deposited onto the completed devices. Two materials deposited by chemical bath deposition are applied as buffer layer, namely either CdS or Zn(O,S).

CdS is deposited in a reactor containing a mixture of the following solutions: 21 cm^3 of ammonia [0.95 M], 15 cm^3 of cadmium acetate [2.63×10^{-3} M] and 15 cm^3 of thiourea [0.05 M], and heated at 60°C; the deposition of 40 nm-thick CdS takes 8 min, starting from precursor solutions at room temperature.

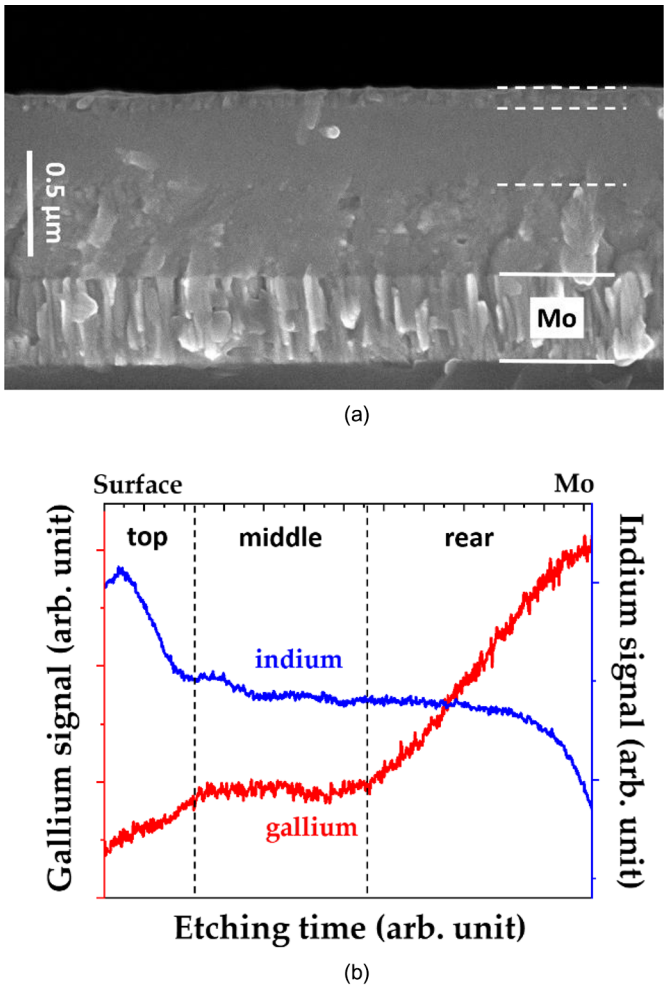

Fig. 2. (a) Scanning electron microscope image of the cross section of the film at the end of the first stage. This image shows the morphological layered structure of the film at the end of the first stage. (b) Qualitative profiles of gallium (in red) and indium (in blue) measured by glow discharge optical emission spectrometry throughout a film at the end of the first stage. This plot shows three different zones corresponding to the layers observed by SEM.

Zn(O,S) is deposited following a recipe described in details within [14]. This fast deposition process implies H_2O_2 additive and takes 6 min.

Both resistive ZnO (40 nm) and ZnO:Al (250 nm) are deposited from ceramic targets by RF-sputtering. Ni (50 nm)/Al(2.5 µm)/Ni(50 nm) stack deposited by e-beam throughout a shadow mask acts as contact grid for 0.5 cm^2 total area cells.

Photovoltaic parameters are extracted from $J(V)$ measurements performed under standard conditions of test (25 °C, Xenon lamp with AMG1.5 optical filter, 1000 W/m^2). For temperature dependent $J(V)$, the sample temperature is varied from 280 K up to 330 K using a Peltier element. External quantum efficiency (EQE) is performed at room temperature using a laboratory built setup; note that the J_{sc} of the best cells is deduced from EQE accounting that grids surface shades 3% of total area.

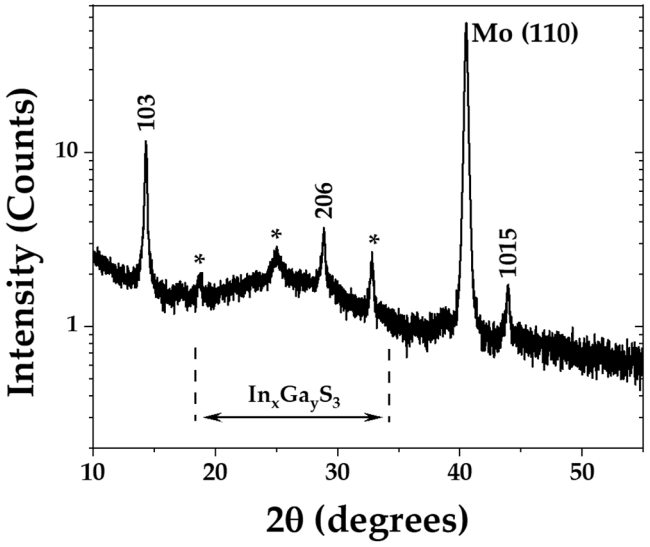

Fig. 3. X-ray diffraction pattern measured from layer at the end of the first stage. The indexed peaks correspond to reflections assigned to β-In_2S_3 structure. The peaks pointed by stars, as well as the broad signal ranging between 18° and 34°, is assigned to $In_xGa_yS_3$ hexagonal/rhombohedral phase.

3 Results and discussion

3.1 Investigation of the film at the end of the 1st-stage

Since the present modified process implies exclusively changes during the first stage, the characteristics of the film achieved at the end of this stage, namely $(In_xGa_y)S_z$, have been firstly extensively investigated.

In Figure 2a is shown an SEM image of the cross section of the film. This picture shows the film, of thickness about 800 nm, appears as being a stack of three layers, each with specific morphological features. The layer closest to the Mo back contact is made of rather narrow grains clearly visible; which contrasts with the intermediate layer appearing much less granular. The third and thinner layer (about 100 nm-thick), homogeneously covering the film, is made of grains which microstructure is visible in the SEM image.

In order to evaluate whether this layered structure evolves along with different compositions, a qualitative depth profile was performed by GDOES. In and Ga signals (no quantification) acquired throughout the film and plotted in Figure 2b also show three areas, referenced to as top/middle/rear in the following. The top, corresponding to the surface of the film, shows an increased(decreased) In (Ga) content as compared to the compositional plateau observed in the middle. Regarding the rear area, it shows a linear increase of Ga signal toward the back contact and a sharp In signal decrease at the vicinity of the back. Interestingly, the evolution of In and Ga signals of rear and middle is consistent with the evaporation fluxes supplied during the first stage; more surprising is the sharp increase of In contribution at the top.

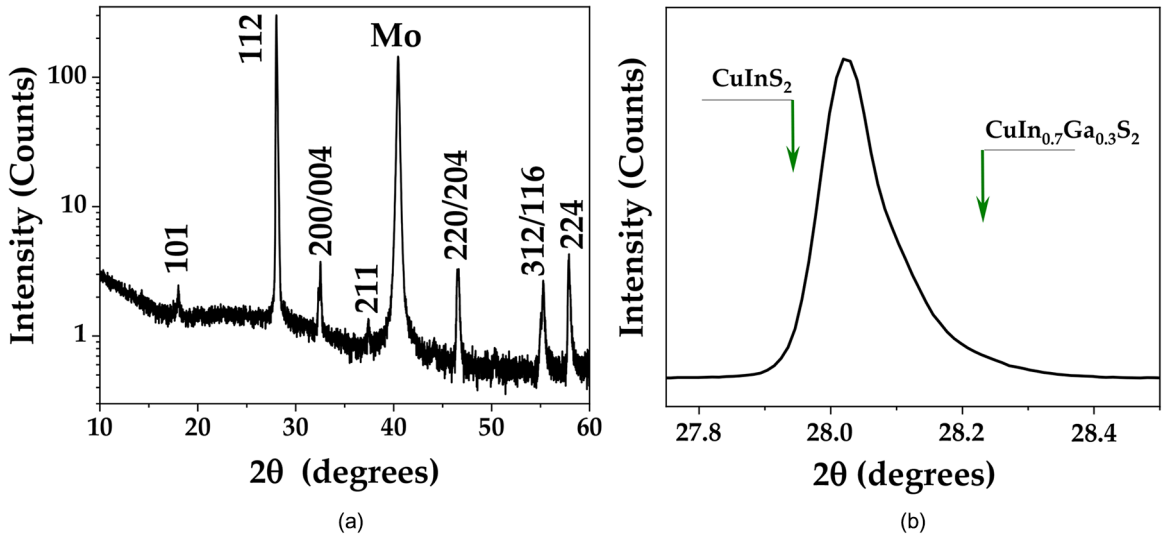

Fig. 4. (a) X-ray diffraction pattern measured from a completed absorber. All of the indexed peaks can be attributed to the chalcopyrite phase of Cu(In,Ga)S_2 (JCPDS#32–0339). (b) Focus on the (112) reflection of the completed absorber. The main contribution is centered at 28.02°, which corresponds to a GGI of 0.11.

This film was further investigated by XRD. The resulting θ/2θ diagram, plotted in Figure 3a, suggests the film contains crystallites of at least two phases, namely tetragonal β-In_2S_3-like and hexagonal/rhombohedral $InGaS_3$-like. In addition, a deeper analysis of the peaks assigned to β-In_2S_3-like reveals two information. First, all peaks are shifted toward larger angles, which suggests a small portion of indium is substituted by gallium within In_2S_3 structure. Second, these peaks do not fit a single contribution; a shouldering toward smaller angles is always detected. This latter observation is consistent with the presence of In_2S_3 with even weaker gallium content somewhere in the film.

To summarize, the film at the end of the first stage is a stack of three layers and contains crystallites which structure corresponds to either tetragonal β-In_2S_3-like or hexagonal/rhombohedral $InGaS_3$-like. The coexistence of these phases can be explained by the low solubility range of gallium sulfide in indium sulfide; Krämer et al. [15] reported single phased $In_{2-2x}Ga_{2x}S_3$ for $0 < x < 0.05$, while for higher x they observed the coexistence of In_2S_3 and $In_xGa_yS_z$ hexagonal/rhombohedral phases. By taking into account the qualitative GDOES profiles shown in Figure 2b, it is probable the $InGaS_3$-like is located at the rear, the β-$In_{2-\delta}Ga_\delta S_3$ with higher δ in the middle and the β-$In_{2-\delta}Ga_\delta S_3$ with the lowest δ at the top.

3.2 Investigation of completed absorber

The films grown following the implemented modified 3-stage process have been investigated by X-Ray diffraction. The diffraction pattern is plotted in Figure 4a. All of the peaks can be attributed to chalcopyrite structure of Cu(In, Ga)S_2 [JCPDS#32-0339]. As illustrated in Figure 4b in the case of (112) peak, all peaks show a strong shouldering towards larger angles. This latter suggests GGI is not constant throughout the completed CIGS layer. Note that the main contribution of peak is centered at 28.02°, which corresponds to a GGI of 0.11.

In order to verify if, similar to the film at the end of the first stage, the completed absorber has layered-like morphology, we performed SEM. Figure 5a depicts a cross sectional view of the completed cell investigated further in the manuscript. This SEM image shows large grains, extended throughout the whole CIGS film and no specific features like smaller grains close to the back contact are visible. Amongst the reasons for such a morphology, one can mention the rather low GGI (0.1 in total) and the rather soft gallium gradients throughout the film, as illustrated by the GDOES profile plotted in Figure 5b. The combination of XRD and GDOES analyses suggest the GGI across the film consist of a large plateau of GGI = 0.11 built in between a top and rear layers of higher GGI (∼ 0.18).

Interestingly, despite the strong GGI gradient observed in the film at the end of the first stage, the completed absorber shows flattened GGI profile. It appears that, in the case of the presently studied films with rather low GGI, absorber completion yields a full redistribution of constituting elements, which was not the case for higher gallium contents [11]. The spatial redistribution leading to the formation of large grains, commonly called recrystallization in the field of pure selenides, is known to be beneficial for the optoelectronic characteristics of the films and consequently for the photovoltaic performance [16]; the arising question is therefore whether one may expect reaching higher efficiencies with this kind of film.

3.3 Investigation of solar cells

Solar cells were prepared from absorbers synthesized following the modified process described in Section 2.1. Firstly, devices with the standard (CBD)CdS buffer layer

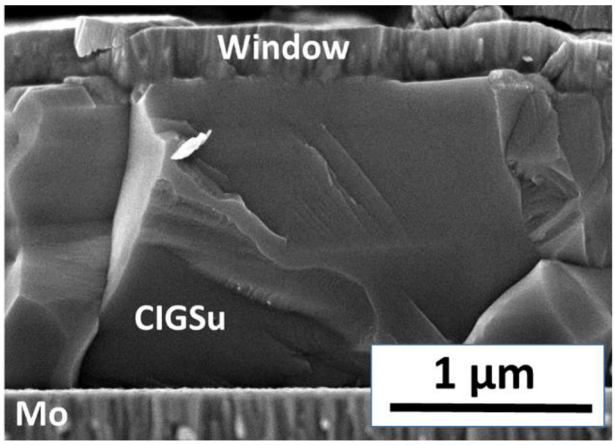

(a)

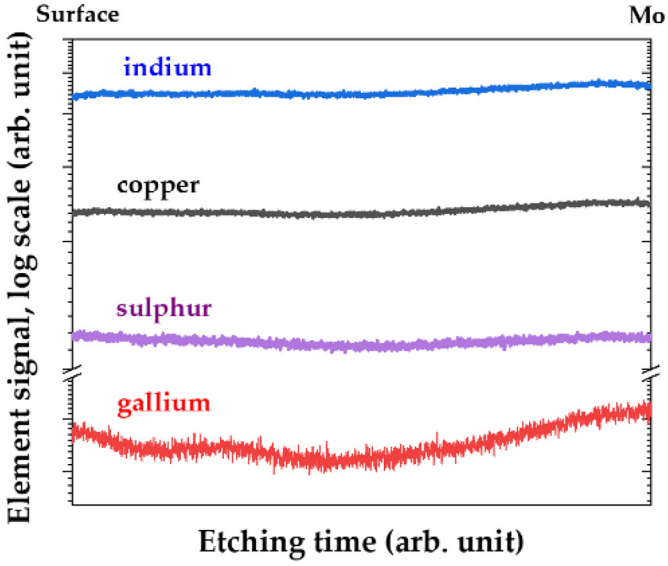

(b)

Fig. 5. (a) Scanning electron microscopy cross sectional image of a solar cell based on $Cu(In,Ga)S_2$ film synthesized following the modified three-stage process investigated herein. (b) Qualitative profiles of gallium (in red), indium (in blue), copper (in black) and sulphur (in violet) measured by glow discharge optical emission spectrometry throughout a completed absorber.

were investigated. The $J(V)$ curve of the best device we fabricated so far is plotted in Figure 6. An efficiency of 16.0% was measured in-house with AR coating. The main improvement, compared with the highest efficiencies reported in the literature [4–6], is undoubtedly the outstanding value of the FF (0.77) for a close to 1.60 eV polycrystalline absorber-based device. Note that the extrapolation to 0 K of $V_{oc}(T)$ gives a value of 1.55 eV, which is very close to that of the bandgap and suggest the dominant recombination mechanism is occurring in the space charge region.

The EQE with AR coating reveals a sharp absorption cut-off at about 800 nm; the EQE derivative fits a Gaussian centered at 1.56 eV. Furthermore, the EQE in the short wavelengths (i.e. 400–525 nm) is strongly penalized by the parasitic absorption of the (CBD)CdS buffer. This issue can be tackled by using the alternative (CBD)Zn(O,S) buffer layer; which bandgap is greater than 3 eV thus optically less harmful in the short wavelengths. In addition, this buffer is reported as yielding more adapted band configuration at the CIGS/buffer interface [17] and thereby possibly leads to higher V_{oc} relative to CdS-buffered device.

Devices with either (CBD)CdS (as reference) or (CBD)Zn(O,S) were prepared from absorbers grown during the same deposition process. The $J(V)$ characteristics of the best devices fabricated are plotted in Figure 7 along with their EQE. These graphs show that the use of (CBD)Zn(O,S) indeed improves EQE in the short wavelengths region, leading to a gain in J_{sc} close to 1 mA/cm^2 and allows achieving higher V_{oc} than (CBD)CdS reference. The counterpart is, for the presented results, a lowered FF which prevents reaching efficiency greater than 16%. The origin of the observed FF loss is not fully clear so far; nevertheless, further understanding will first need to

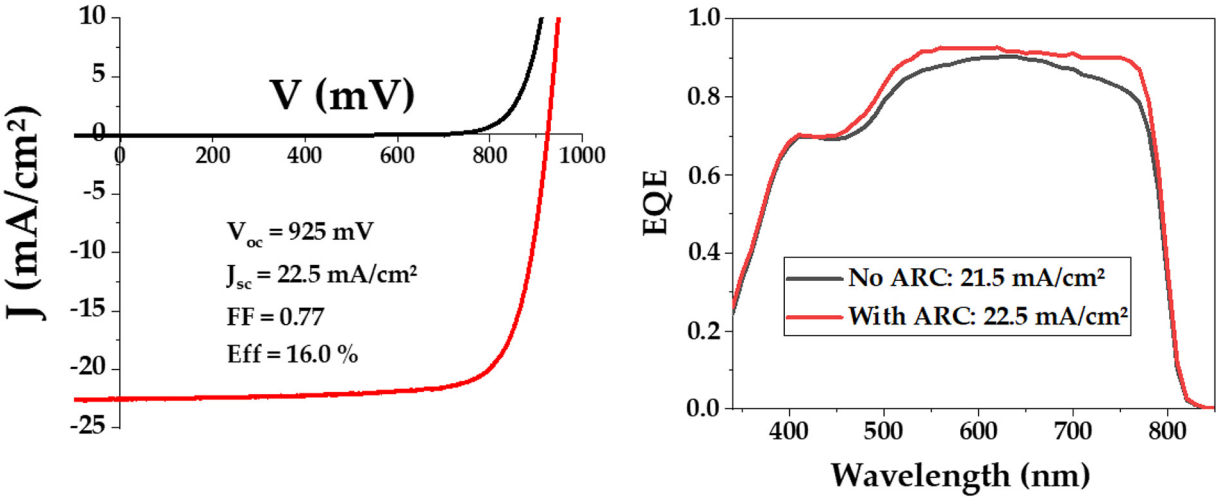

Fig. 6. *JV* characteristic of the best solar cell buffered with (CBD)CdS. Inset are presented the photovoltaic parameters deduced from the *JV* curve and the EQE (with ARC).

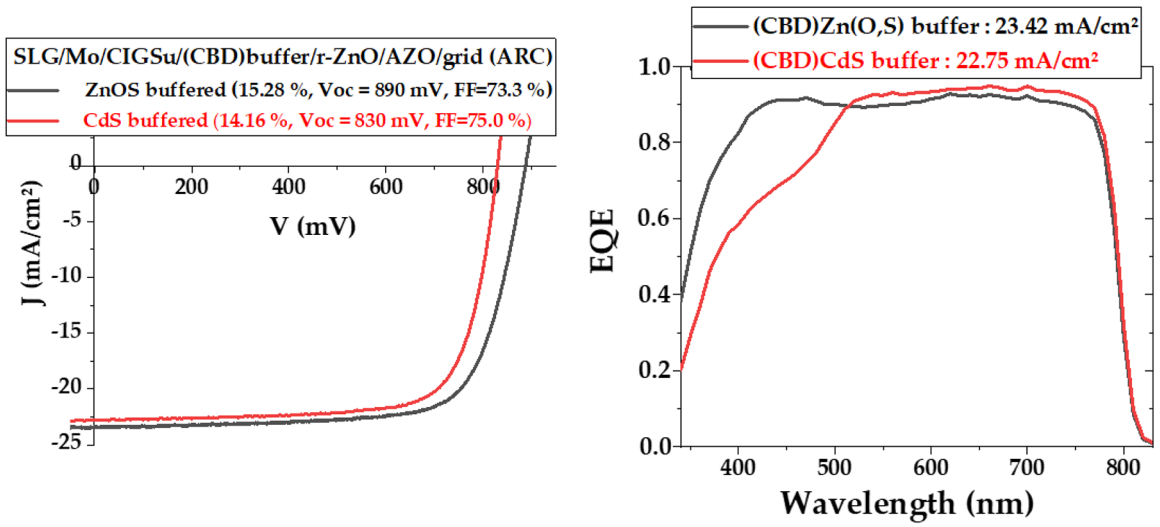

Fig. 7. *JV* characteristics and EQE (with ARC) of the best solar cell buffered with either (CBD)CdS (in red) or with (CBD)Zn(O,S) (in black).

optimize the Zn(O,S) deposition conditions along with the adaptation of the window layer as suggested recently by Sood et al. [18].

4 Conclusions

In the present study we have investigated the characteristics of $Cu(In,Ga)S_2$ films grown following a modified three stage process consisting in decreasing(increasing) flux of gallium(indium) during the first stage. The resulting In-Ga-S film exhibits a layered structure with β-In_2S_3-like containing low amount of gallium near the surface and $In_xGa_yS_3$-like hexagonal phase near the back contact. The low gallium content of the upper half of the film appears beneficial for the formation of $Cu(In,Ga)S_2$ absorber with grains extended throughout the whole absorber thickness. The devices fabricated from these films achieve outstanding performance of 16.0% when buffered with (CDB)CdS and completed with standard ZnO/ZnO:Al window. To further increase the efficiency, devices buffered with (CBD) Zn(O,S) were investigated. On the one hand, both the output voltage and the current density are increased thanks to improved band configuration at CIGS/buffer interface and improved EQE in the short wavelengths, respectively. On the other hand, the fill factor is lowered, probably because of the non-optimal band structure at the buffer/window interface. Consequently, the efficiency reached herein with (CBD)Zn(O,S) buffer does not exceed 15.3%. Important work remains to optimize Zn(O,S)/ window characteristics and thereby fully benefit of the potential of those absorbers.

The outstanding performance achieved should nevertheless not blind both the remaining rather low V_{oc} of the devices, and the fact that the bandgap of the absorber remains about 1.55 eV, which is slightly too low for being applied as top cell in tandem devices. Increasing the Ga amount supplied during the first stage is assuredly the most obvious way to increase the absorber bandgap up to the optimal value of 1.7 eV. However, the present conclusions emphasize that higher amount of Ga would hinder the recrystallization of the whole film and thereby yield degraded optoelectronic properties of the absorber, thus photovoltaic performance. As a conclusion, the community of Cu(In,Ga)S_2 growers should continue exploring alternative deposition strategies to overcome that issue.

This research work was supported by the French ANR-EPCIS Project (Grant No. ANR-20-CE05-0038) and the PIA (Grant no. ANR-IEED-002-01).

Author contribution statement

Experiments were conducted by N. Barreau, E. Bertin, A. Crossay and L. Assmann. The supervision of the project was ensured by N. Barreau, O. Durand, E. Gautron and D. Lincot. Discussion on results were conducted by N. Barreau, L. Arzel, S. Harel and Th. Lepetit. The writing of the manuscript was coordinated by N. Barreau and proof reading done by all co-authors.

References

1. M. Bär, W. Bohne, J. Röhrich, E. Strub, S. Lindner, M.C. Lux-Steiner, Ch.-H. Fischer, T.P. Niesen, F. Karg, Determination of the band gap depth profile of the penternary Cu$(In_{(1-x)}Ga_x)(S_ySe_{(1-y)})_2$ chalcopyrite from its composition gradient, J. Appl. Phys. **96**, 3857 (2004)
2. P. Jackson, R. Wuerz, D. Hariskos, E. Lotter, W. Witte, M. Powalla, Effects of heavy alkali elements in Cu(In,Ga)Se_2 solar cells with efficiencies up to 22.6%, Phys. Stat. Solidi RRL. **10**, 583 (2016)
3. M. Nakamura, K. Yamaguchi, Y. Kimoto, Y. Yasaki, T. Kato, H. Sugimoto, Cd-free Cu(In,Ga)$(Se,S)_2$ thin-film solar cell with record efficiency of 23.35%, IEEE J. Photovolt. **9**, 1863 (2019)
4. H. Hiroi, Y. Iwata, S. Adachi, H. Sugimoto, A. Yamada, New world-record efficiency for pure-sulfide Cu(In,Ga)S_2 thin-film solar cell with Cd-free buffer layer via KCN-free process, IEEE J. Photovolt. **6**, 760 (2016)
5. S. Shukla, M. Sood, D. Adeleye, S. Peedle, G. Kusch, D. Dahliah, M. Melchiorre, G.-M. Rignanese, G. Hautier, R. Oliver, S. Siebentritt, Over 15% efficient wide-band-gap Cu(In,Ga)S_2 solar cell: suppressing bulk and interface recombination through composition engineering, Joule 5, 1816 (2021)
6. N. Barreau, A. Thomere, D. Cammilleri, A. Crossay, C. Guillot-Deudon, A. Lafond, N. Stephant, D. Lincot, M.T. Caldes, R. Bodeux, B. Berenguier, High efficiency solar cell based on Cu(In,Ga)S_2 thin film grown by 3-stage process, in *2020 47th IEEE Photovoltaic Specialists Conference (PVSC)*, IEEE, Calgary, OR (2020), pp. 1715
7. R. Kaigawa, K. Funahashi, R. Fujie, T. Wada, S. Merdes, R. Caballero, R. Klenk, Tandem solar cells with Cu(In,Ga)S_2 top cells on ZnO coated substrates, Sol. Energy Mater. Solar Cells **94**, 1880 (2010)
8. S. Merdes, R. Mainz, J. Klaer, A. Meeder, H. Rodriguez-Alvarez, H.W. Schock, M.Ch. Lux-Steiner, R. Klenk, 12.6% efficient CdS/Cu(In,Ga)S_2-based solar cell with an open circuit voltage of 879mV prepared by a rapid thermal process, Solar Energy Mater. Solar Cells **95**, 864 (2011)
9. A. Thomere, C. Guillot-Deudon, M.T. Caldes, R. Bodeux, N. Barreau, S. Jobic, A. Lafond, Chemical crystallographic investigation on Cu_2S-In_2S_3-Ga_2S_3 ternary system, Thin Solid Films **665**, 46 (2018)
10. N. Barreau, Indium sulfide and relatives in the world of photovoltaics, Solar Energy **83**, 363 (2009)
11. A. Thomere, N. Barreau, N. Stephant, C. Guillot-Deudon, E. Gautron, M.T. Caldes, A. Lafond, Formation of Cu(In,Ga)S_2 chalcopyrite thin films following a 3-stage co-evaporation process, Solar Energy Mater. Solar Cells **237**, 111563 (2022)
12. A.M. Gabor, J.R. Tuttle, D.S. Albin, M.A. Contreras, R. Noufi, A.M. Hermann, High-efficiency $CuIn_xGa_{1-x}Se_2$ solar cells made from $(In_x,Ga_{1-x})_2Se_3$ precursor films, Appl. Phys. Lett. **65**, 198 (1994)
13. J. Kessler, J. Scholdstrom, L. Stolt, Rapid Cu(In, Ga)Se_2 growth using "end point detection" in: Conference Record of the *Twenty-Eighth IEEE Photovoltaic Specialists Conference* - F 2000 F (Cat. S No.00CH37036), IEEE, Anchorage, AK, USA, 2000: pp. 509. https://doi.org/10.1109/PVSC2000.915883.
14. M. Buffière, S. Harel, L. Arzel, C. Deudon, N. Barreau, J. Kessler, Fast chemical bath deposition of Zn(O,S) buffer layers for Cu(In,Ga)Se_2 solar cells, Thin Solid Films. **519**, 7575 (2011)
15. V. Kramer, R. Nitsche, J. Ottemann, New single-crystalline phases in the system Ga_2S_3-In_2S_3, J. Crystal Growth **7**, 285 (1970)
16. N. Barreau, T. Painchaud, F. Couzinié-Devy, L. Arzel, J. Kessler, Recrystallization of CIGSe layers grown by three-step processes: a model based on grain boundary migration, Acta Mater. **58**, 5572 (2010)
17. M. Sood, J. Bombsch, A. Lomuscio, S. Shukla, C. Hartmann, J. Frisch, W. Bremsteller, S. Ueda, R.G. Wilks, M. Bär, S. Siebentritt, Origin of interface limitation in Zn(O,S)/$CuInS_2$-based solar cells, ACS Appl. Mater. Interfaces **14**, 9676 (2022)
18. M. Sood, P. Gnanasambandan, D. Adeleye, S. Shukla, N. Adjeroud, R. Leturcq, S. Siebentritt, Electrical barriers and their elimination by tuning (Zn,Mg)O composition in Cu(In,Ga) S_2: systematic approach to achieve over 14% power conversion efficiency (2022), arXiv: 2202.10708

Cite this article as: Nicolas Barreau, Eugène Bertin, Alexandre Crossay, Olivier Durand, Ludovic Arzel, Sylvie Harel, Thomas Lepetit, Lionel Assmann, Eric Gautron, Daniel Lincot, Investigation of co-evaporated polycrystalline Cu(In,Ga)S_2 thin film yielding 16.0% efficiency solar cell, EPJ Photovoltaics **13**, 17 (2022)